

Damage analysis of cut-and-cover tunnel structures under seismic loading

Tae-Hyung Lee¹ · Duhee Park² · Duy Duan Nguyen¹ · Jeong-Seon Park²

Received: 13 April 2015 / Accepted: 10 October 2015
© Springer Science+Business Media Dordrecht 2015

Abstract Damage analyses of rectangular cut-and-cover tunnels are performed to define the damage states and corresponding damage indices (DIs) under seismic loading. Single, double, and triple box structures designed for metro subway systems in South Korea are used. The tunnel structures are modeled by nonlinear frame elements attached to a series of normal and shear springs to simulate the soil–tunnel interaction. Pushover analyses are performed to develop the capacity curves and to monitor the development of plastic hinges. Parallel elastic analyses are also performed to determine the elastic moments at which plastic hinges form. For each tunnel and site condition, three damage states, which are minor, moderate, and extensive, are defined in terms of number of plastic hinges that form at the corners of the tunnel structure. Each damage state is linked to the corresponding DI, which is defined as the ratio of the elastic moment to the yield moment and free-field shear strain. DI for the single box tunnel is shown to be mostly independent of the shear wave velocity of soil. The values of DIs for single, double, and triple box tunnels range from 1.0 to 2.0. It is highlighted that the proposed damage state associated with DI and shear strain provide an enhanced estimate of the seismically induced damage of box tunnels and can be easily utilized in a performance-based design.

Keywords Cut-and-cover tunnel · Seismic design · Damage analysis · Inelastic frame analysis · Damage state · Damage index

✉ Duhee Park
dpark@hanyang.ac.kr

¹ Department of Civil Engineering, Konkuk University, Seoul, Korea

² Department of Civil and Environmental Engineering, Hanyang University, Rm 506 Jaesung Civil Eng Bldg., Wangsimni-ro 22, Sungdong-gu, Seoul 133-791, Korea

1 Introduction

Underground structures are known to be less vulnerable to earthquake induced damage compared to structures built above-ground (Dowding and Rozan 1978). However, strong earthquakes have shown that even underground structures can suffer significant structural damage under severe seismic excitation (Hashash et al. 2001). The tunnel damage pattern has been identified through various case studies (Dowding and Rozan 1978; Hashash et al. 2001; Owen and Scholl 1981; Sharma and Judd 1991; Wang 1985). Nakamura et al. (1996) presents a detailed report on the damage of Daikai station during the 1995 Kobe earthquake. Wang et al. (2001) provides an extensive analysis of damage observed in mountain tunnels during the 1999 Chi–Chi earthquake. Wang and Zhang (2013) classify the seismic damage of mountain tunnels, which is validated through 2008 Wenchuan earthquake. Considering the important roles that underground structures play in modern urban areas, accurate evaluation of the seismic performance of underground structures is critical for ensuring sustainability.

Since underground structures are completely enclosed within the ground and cannot vibrate freely, they conform to the ground movement. Therefore, a pseudo-static analysis, where the free-field horizontal displacement profile calculated from a one-dimensional site response analysis is imposed to the ground surrounding the tunnel, is most often performed in practice. It ignores the dynamic interaction between the tunnel and the ground. Analytical pseudo-static methods for calculating tunnel response under vertically propagating shear waves have been presented (Bobet 2003; Hashash et al. 2001; Huo et al. 2006; Park et al. 2009; Penzien 2000; Wang 1993). Pseudo-static numerical analyses are also widely performed in practice (Hashash et al. 2001, 2005; Wang 1993). Dynamic analyses were also performed to simulate the dynamic underground structure–soil interaction. Several studies compared the pseudo-static and dynamic analyses of underground structures. Hashash et al. (2010) compared the calculated racking ratio (R) of pseudo-static and dynamic analyses for box structures with flexibility ratio (F) ranging from less than 1 up to 12. R is defined as the ratio of the relative displacement between the top and bottom corners of the structure to the free field relative displacement. F represents the relative flexibility between the structure and the soil. If $F < 1$, the structure is stiffer than the surrounding soil, whereas the soil is stiffer than the structure if $F > 1$. The results were almost identical for single boxes. For double box tunnels, R calculated from dynamic analysis were shown to be up to 25 % higher than those determined from pseudo-static analyses. Argyroudis and Ptilakis (2012) also compared pseudo-static and dynamic analysis results of underground structures. They concluded that the difference between the pseudo-static and dynamic analyses is not significant, and the pseudo-static analysis provides sufficiently accurate estimate of the dynamic response tunnels.

To overcome the evident limitations of an elastic analysis, studies employing nonlinear models for the underground structure have been carried out. A pushover analysis of Daikai subway station during the Kobe earthquake 1995 was executed by Liu and Liu (2008) through inelastic finite element analysis to identify the failure mechanism of the double rectangular tunnel. The study showed that the tunnel fails due to the development of plastic hinges in the weak center column, which led to collapse of the column and the upper slab. Andreotti et al. (2013) performed pseudo-static analysis of horseshoe shaped tunnels using the finite difference approach. Elastic beams with six plastic hinges represent tunnel lining and damage states were defined based on the number of plastic hinges. Because the numerical model pre-assigns the location of plastic hinges, it cannot accurately model the

propagation of the plastic hinges during seismic loading. Khani and Homami (2014) performed pushover analyses on a one bay and two story rectangular tunnel. From the analysis results, the capacity curve of the double-stacked box was proposed.

Previous studies deal with specific sites and tunnels. For performance-based design, there is a need to define the failure mechanisms for different types of tunnels, a wide range of soil profiles, and ground motion intensities based on damage analyses. In addition, representative damage states of tunnels and associated quantitative indices need to be characterized. Argyroudis and Pitilakis (2012) proposed four damage states for circular and rectangular tunnels, which are minor/slight, moderate, extensive, and collapse. Each damage state was linked to the damage index (DI), which is defined as the ratio of elastic moment (M) to resisting design moment (M_d). However, since damage analyses were not performed, representative damage indices (M/M_d) were assumed without a clear engineering rationale.

In this study, we investigate the accumulation of damage of rectangular single-story cut-and-cover tunnels under seismic loading from pseudo-static inelastic frame analysis and present a new criterion for defining the damage states. Three types of single-story box structures, which are single, double, and triple box tunnels, were modeled. The tunnels were modeled with a series of nonlinear beam-column elements to capture the development and evolution of plastic hinges. Each damage state defined in this study is associated with the DI proposed by Argyroudis and Pitilakis (2012). The damage indices of single, double, and triple tunnels for various soil conditions are compared. Representative free-field shear strains for each damage state are also presented.

2 Site conditions and tunnel sections

We modeled three types of rectangular box structures, of which the cross-sectional dimensions are depicted in Fig. 1. Single, double, and triple boxes shown are actual cut-and-cover metro tunnels designed and built in South Korea. For simplicity, tunnels were assumed to be located within a uniform soil layer. The depth of overburden was 7 m for all tunnels, as shown in Fig. 1. K_0 of 0.5 was assumed for all profiles. Both the center-to-center width and height were 6.0 m for each box. The thickness of ceiling slab, walls, and bottom slab was 1.0 m. For the double and the triple boxes, the cross-sectional dimension

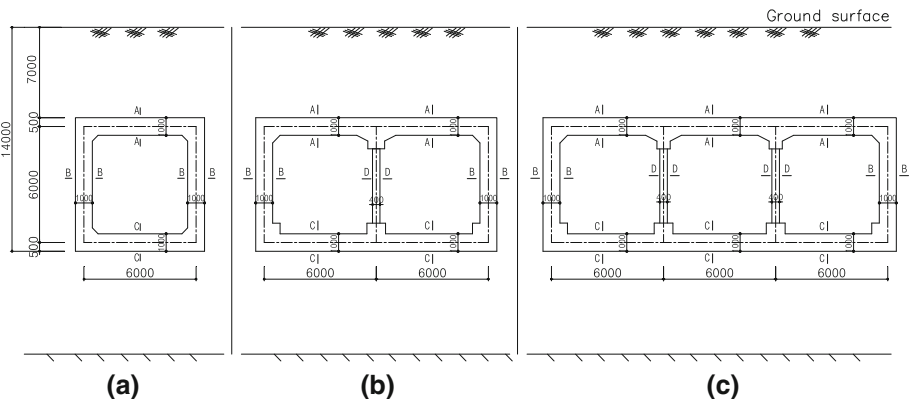


Fig. 1 Cross sections of cut-and-cover tunnels: **a** single tunnel, **b** double tunnel and **c** triple tunnel

of the interior column was 0.4 m by 1.0 m. The cross-sectional dimensions of structural members including reinforcement details are depicted in Fig. 2. The nominal compressive strength of concrete (f'_c) used was 27.5 MPa, while the nominal yield strength of the reinforcing steel (f_y) assigned was 413 MPa.

3 Numerical modeling

To evaluate the capacity of the box tunnels, we performed a series of pseudo-static analyses. Dynamic analyses were not performed because the difference between pseudo-static and dynamic analyses was shown to be not significant, as explained previously. A continuum analysis was not used because it was demonstrated that the difference between a frame and continuum analyses is not pronounced if the spring coefficients are selected appropriately (Chang et al. 2014). Only the racking of the rectangular tunnel was simulated, because it is the critical mode of deformation in most cases.

Finite element models of three tunnels were developed within the capability of SAP2000 (ver. 15), a commercial program. Each structural member of the tunnel, namely ceiling slab, wall, bottom slab, and interior column, was modeled using frame elements with joint-offset feature at the corner of tunnels to reflect the rigidity of the wall-slab joint connection. We used conventional line-type elements based on the Euler–Bernoulli beam theory using a cubic shape function for the displacement interpolation. The number of

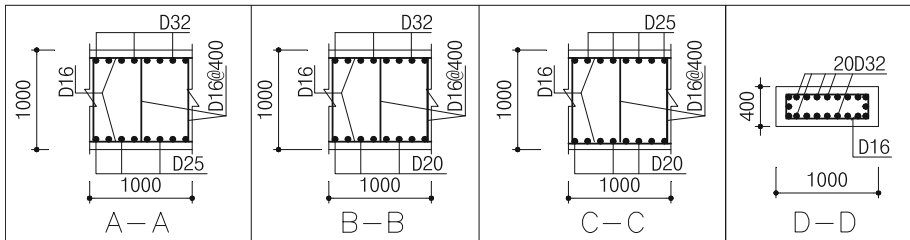


Fig. 2 Dimensions and reinforcement details of structural members

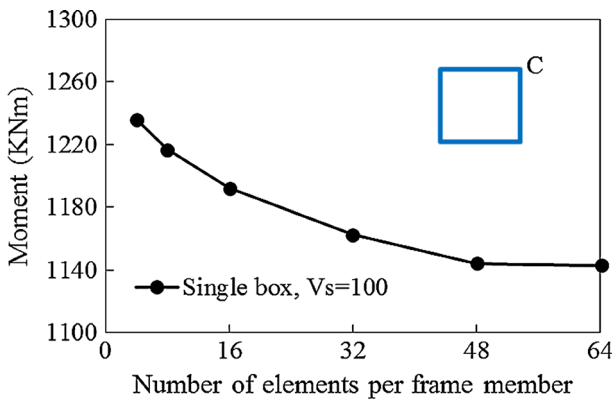


Fig. 3 Convergence of the bending moment at location C with increase in the number of elements per structural member

elements was determined from mesh convergence analysis, as shown in Fig. 3. The bending moment at top right corner (location C) of the single box is shown to converge when 48 elements are used. We used 64 elements per structural member in all analyses. Because Euler–Bernoulli beam elements were used, shear failure of the structural member was not allowed. Even though a flexural failure is expected considering the slenderness of the walls and slabs, future studies are needed to investigate the possibility of shear failure.

A plastic hinge model was used for all frame elements, not only to capture the nonlinear behavior of the tunnel, but also to capture the propagation of plastification along the length of the structural members. The behavior of the plastic hinge, which is located at each end of a frame element, is dictated by the section model, namely the nonlinear moment–curvature relation. The nonlinear section model was determined by the section analysis for each cross section using nonlinear material models. Material behaviors of concrete and reinforcing steel are dictated by the nonlinear stress–strain relationships as shown in Fig. 4. The elastic moduli of concrete and reinforcing steel used were 24.8 and 200 GPa, respectively. The moment–curvature relationships of sections A–A and D–D are presented in Fig. 5 for an illustrative purpose.

The surrounding soil was modeled by a series of springs in the normal and the shear directions to simulate the soil–tunnel interaction. The spring constants were determined by the procedure specified in the Seismic design code for metropolitan subway of Korea (MLTM 2009). According to the design code, the spring constants of horizontal (K_H) and vertical (K_V) subgrade reactions are defined as

$$K_H = k_{h0} \left(\frac{h}{30} \right)^{-3/4} \tag{1}$$

$$K_V = k_{h0} \left(\frac{b}{30} \right)^{-3/4} \tag{2}$$

where $k_{h0} = \left(\frac{1}{30} \right) E_D$, h and b are the height and the width of the tunnel, respectively, E_D is dynamic elastic modulus. The shear springs for vertical and horizontal frames, K_{SS} and K_{SB} respectively, are defined as

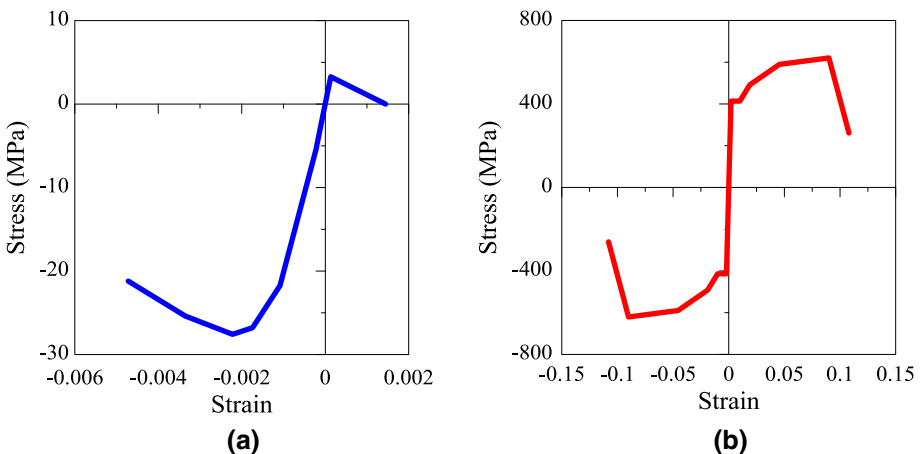


Fig. 4 Material model: **a** concrete and **b** steel

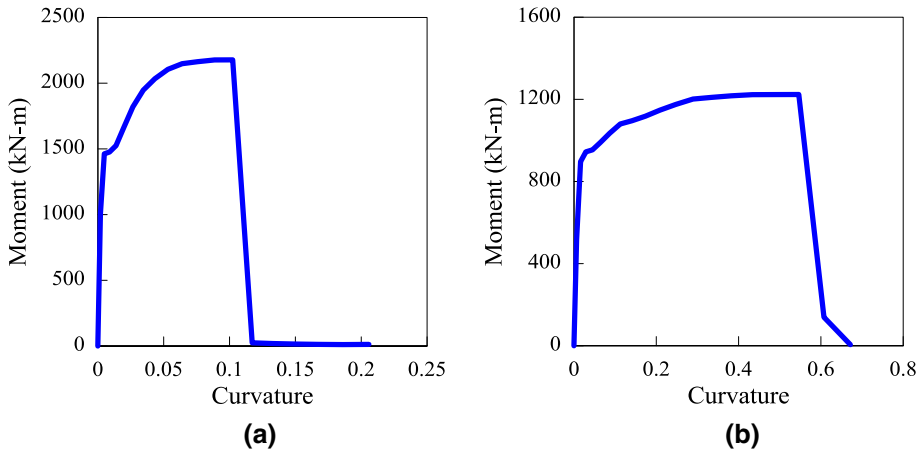


Fig. 5 Moment–curvature relations: **a** section A–A and **b** section D–D

$$K_{SS} = \frac{1}{4} K_H \quad (3)$$

$$K_{SB} = \frac{1}{4} K_V \quad (4)$$

We used the guidelines outlined in Iai (2005) to perform the pseudo-static analyses. Figure 6 shows the boundary conditions, applied forces, and displacements. Firstly, the geostatic forces were applied to the normal springs. Secondly, the free-field soil displacements were applied to the normal springs. The deformation at the top of the structure was applied to the shear springs. In addition, the shear stress induced at the soil-interface was imposed directly on the structure.

In a typical pseudo-static analysis, a one-dimensional (1D) site response analysis is performed to determine the free-field shear strain and horizontal displacement profile. We assumed that the shear strain is uniform within the site profile, and therefore the horizontal displacement was applied as an inverted triangle that decreases linearly with depth. Nonlinear static analysis procedure, also known as the pushover analysis, was performed by continuously increasing the deformation. From the pushover analysis, the base shear–shear deformation curve, development of plastic hinges, and the changes in the bending moment distribution were monitored. The analyses were performed on soils of various shear wave velocities, which were 50, 100, 200, 300, and 400 m/s.

4 Calculated tunnel response

In this section, nonlinear behaviors of three tunnels are discussed in detail. Development of plastic hinges, collapse mechanisms, and parallel elastic analysis results are presented herein.

4.1 Capacity curves of the tunnels

The capacity curve is expressed as a force–deformation relationship, most commonly the base shear versus top displacement in case of a structural system. It is a useful tool to

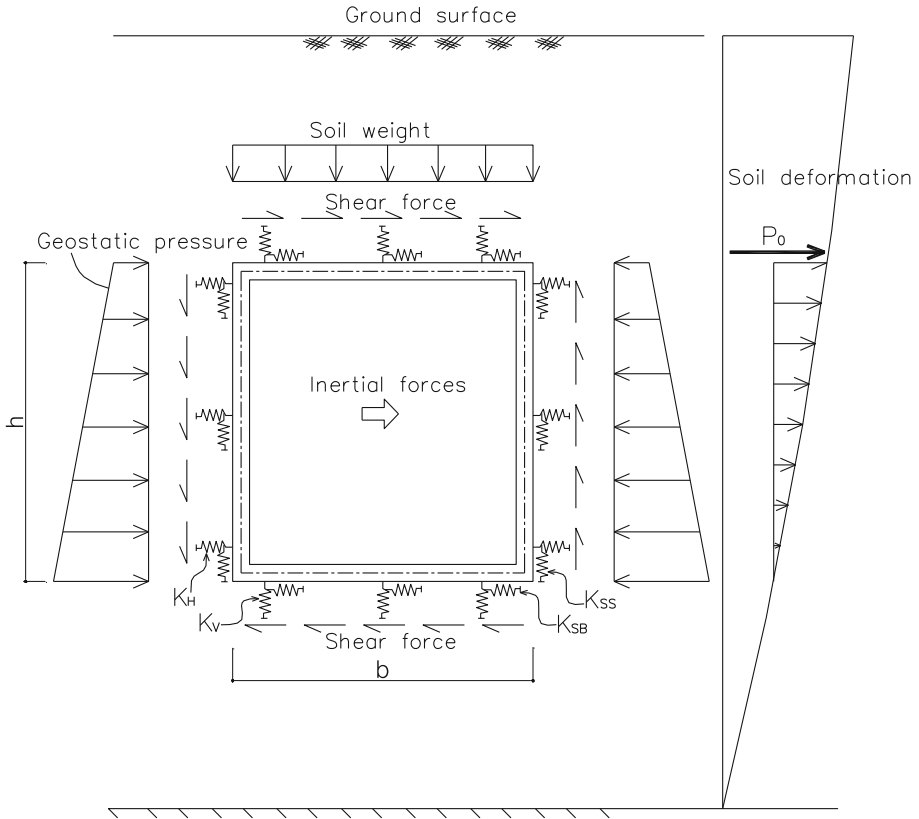


Fig. 6 Boundary conditions and applied loads to the box

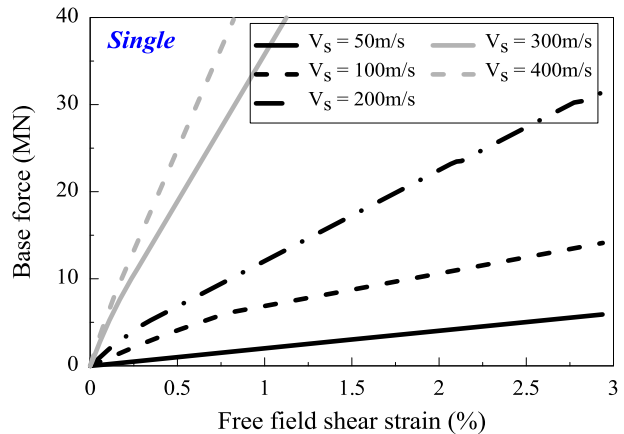
evaluate both the strength capacity and the ductility of the structure. In this study, the capacity curve is expressed as the base force (total lateral force) versus the free field shear strain.

4.1.1 Single box

Figure 7 shows the capacity curves of the single box tunnel for various soil properties. It is observed that a softer soil (with a lower shear velocity) yields a larger free field shear strain of the tunnel. It is attributed to difference in the rigid body rotation of the tunnel and resisting support from the soil spring. A soft soil allows a larger rigid body rotation and a larger shear deformation of the tunnel simultaneously compared to a stiffer soil.

Figure 8 shows the capacity curves and the development of plastic hinges for all soil conditions, where red circles indicate plastic hinges. If the single box is an above-ground structure which stands freely, plastic hinges at four different corners would form a collapse mechanism. However, none of the single box tunnels shows the collapse behavior after four plastic hinges are developed as shown in Fig. 8. Even though the single box tunnel is in an unstable state from the structural point of view, the surrounding soil supports the tunnel and prevents it from collapsing.

Fig. 7 The capacity curves of the single tunnel



4.1.2 Double box

Figure 9 shows the capacity curves of the double box tunnel for various soil properties. Similarly to the case of the single box tunnel, it is observed that a softer soil (with a smaller shear velocity) yields a larger free field shear strain. Figure 10 shows the development of plastic hinges for the cases of $V_s = 50$ m/s and $V_s = 400$ m/s. The double box tunnel does not collapse even after developing plastic hinges at six different corners including both ends of the interior column. It is because the surrounding soil supports the tunnel and prevents it from collapsing, similarly to the case of the single box tunnel. It is observed that the plastic hinges at the interior column do not form until the plastic hinges at the four corners of the outer frame form. The stiffness of the interior column is much smaller than the other structural element as shown in Fig. 2 and the applied forces are mostly resisted by strong elements, which lead to the development of plastic hinges. After plastic hinges are formed at all four corners, the bending moments are redistributed and induce increments of moments at the interior columns until eventually plastic hinges are formed. It is interesting to note that the 6th plastic hinge forms immediately after the 5th plastic hinge develops. In other words, after forming 5th plastic hinge, the box tunnel may suddenly reach an unstable state once a plastic hinge is developed in the interior column.

A hypothetical collapse mechanism is a flexural failure of the ceiling slab after losing the axial capacity of the interior column, as Daikai subway station collapsed during the Kobe earthquake (Liu and Liu 2008; Parra-Montesinos et al. 2006). A number of studies showed that the axial capacity of the reinforced concrete column is reduced once the column loses the flexural capacity (An and Maekawa 1997; Moehle et al. 2002; Yoshimura et al. 2004). However, such failure mechanism cannot be simulated in this study due to the limitation of the modeling scheme adopted herein. A special element that can simulate the reduction of the axial capacity as the element loses its flexural capacity is required to simulate the hypothetical failure mechanism involving the collapse of the ceiling slab.

4.1.3 Triple box

Figure 11 shows the capacity curves of the triple box tunnel for various soil properties. Similarly to the cases of the single box and double box tunnels, it is observed that a softer soil (with a smaller shear velocity) yields a larger free field shear strain of the tunnel.

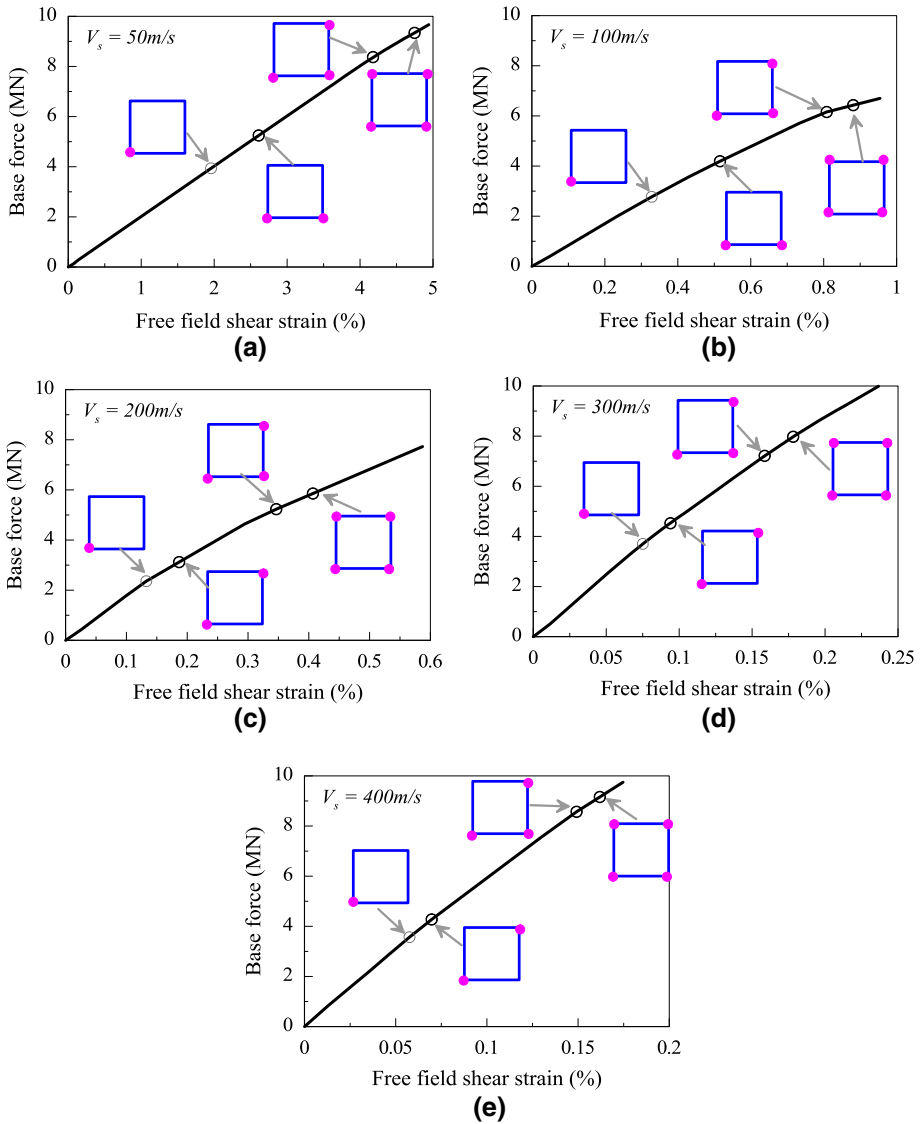
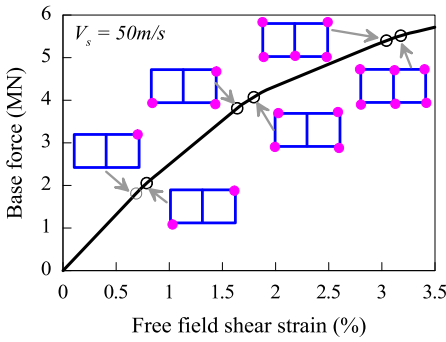
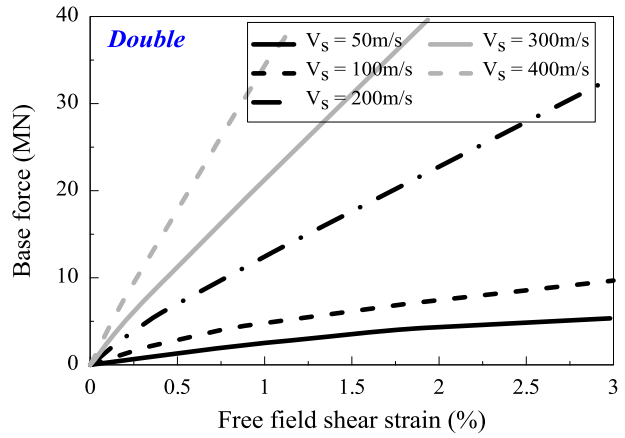


Fig. 8 Development of plastic hinges for single tunnel: **a** $V_s = 50\text{ m/s}$, **b** $V_s = 100\text{ m/s}$, **c** $V_s = 200\text{ m/s}$, **d** $V_s = 300\text{ m/s}$ and **e** $V_s = 400\text{ m/s}$

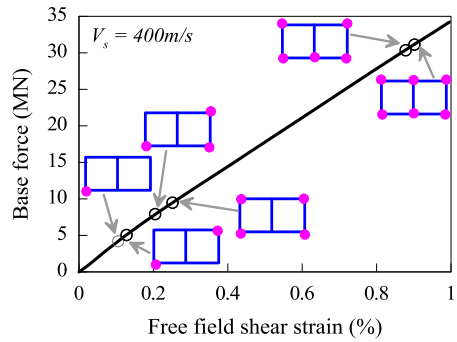
Figure 12 shows the development of plastic hinges for the case of $V_s = 50\text{ m/s}$ and $V_s = 400\text{ m/s}$.

It is again observed that the plastic hinges at the interior columns form after hinges develop at all four outer corners. We may conclude that the interior columns play an important role in the collapse capacity of multiple box tunnels. As in the case of the double box tunnel, the 5th to the 8th plastic hinges are very closely spaced, indicating that the triple box may become unstable immediately after a plastic hinge develops in the interior column.

Fig. 9 The capacity curves of the double tunnel



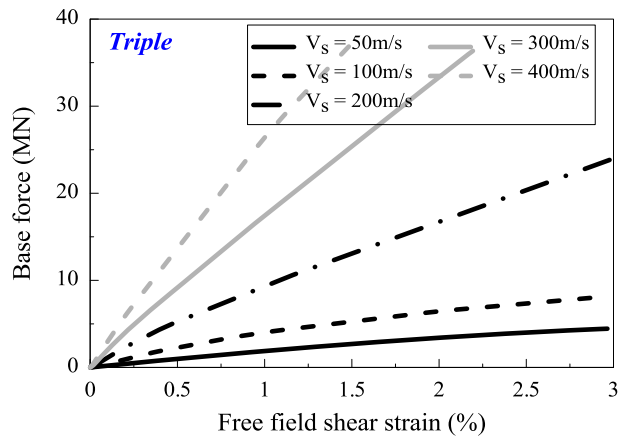
(a)



(b)

Fig. 10 Development of plastic hinges for double tunnel: **a** $V_s = 50$ m/s and **b** $V_s = 400$ m/s

Fig. 11 The capacity curves of the triple tunnel



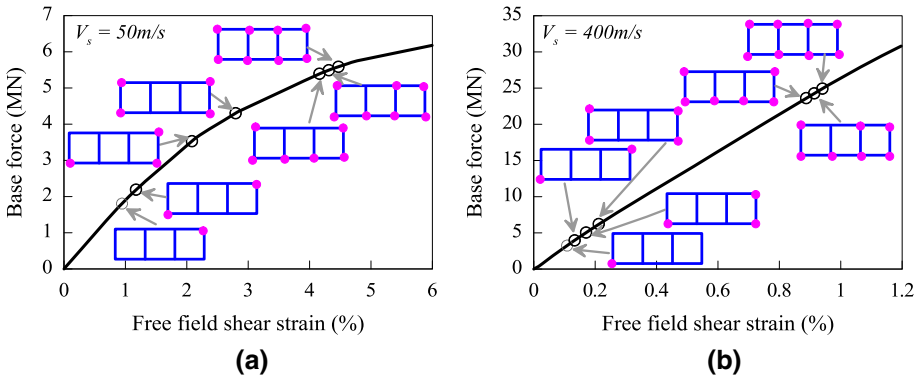
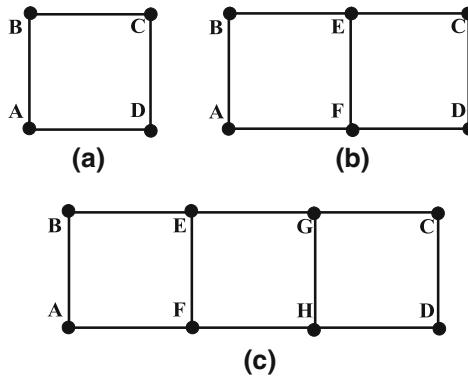


Fig. 12 Development of plastic hinges for triple tunnel: **a** $V_s = 50$ m/s and **b** $V_s = 400$ m/s

4.1.4 Sequence of the plastic hinge formation

The sequences of the development of plastic hinges for single, double, and triple boxes are presented in Fig. 13. It is observed that the sequences of the development of plastic hinges are different for different soil conditions for each of the single box, double box, and triple box cases. For the single box tunnel, the plastic hinge develops at the position A followed by D or C. The fourth plastic hinge develops at position B. It should be noted that the



Tunnel type	Soil conditions				
	$V_s = 50$ m/s	$V_s = 100$ m/s	$V_s = 200$ m/s	$V_s = 300$ m/s	$V_s = 400$ m/s
Single box	A-D-C-B	A-D-C-B	A-C-D-B	A-C-D-B	A-C-D-B
Double box	C-A-D-B-F-E	A-C-D-B-F-E	A-C-D-B-F-E	A-C-D-B-F-E	A-C-D-B-F-E
Triple box	C-A-D-B-F-H-G-E	C-A-D-B-F-H-G-E	A-C-D-B-H-G-E-F	A-C-D-B-H-F-E-G	A-C-D-B-H-F-G-E

Fig. 13 Locations of possible hinges and sequence of plastic hinge formation

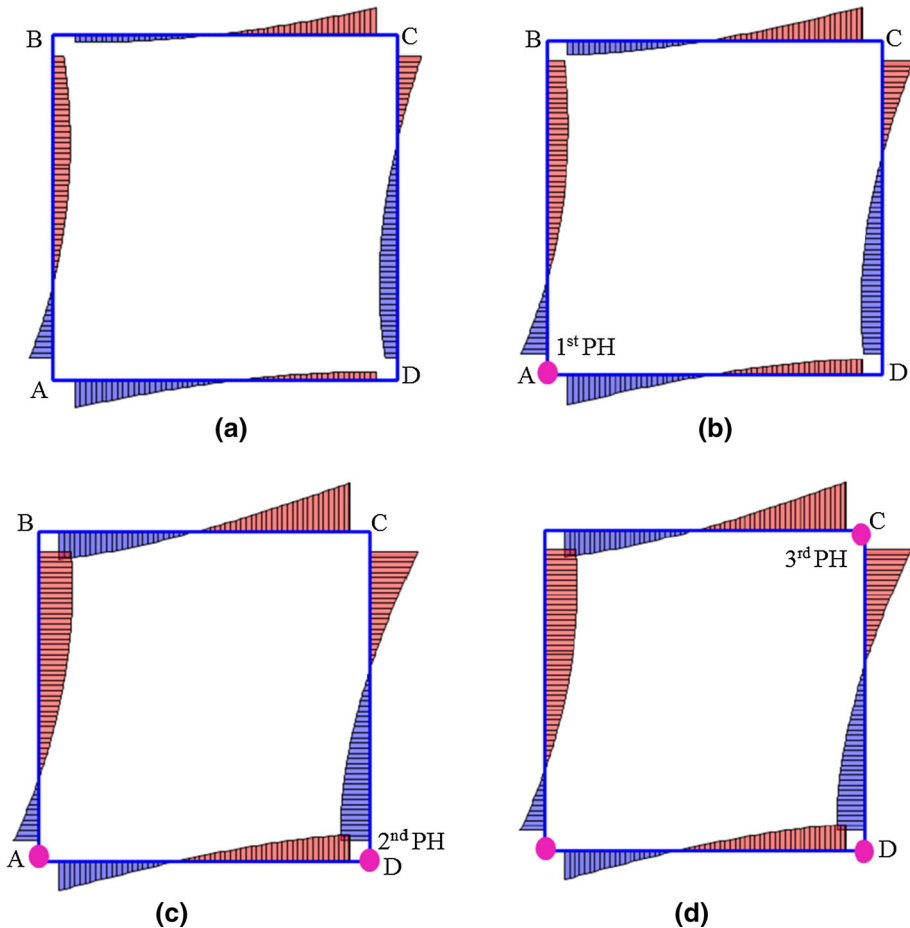


Fig. 14 Bending moment diagrams of single box tunnel, $V_s = 50$ m/s. **a** Elastic range, **b** after 1st plastic hinge is formed, **c** after 2nd plastic hinge is formed, **d** after 3rd plastic hinge is formed

lateral load is applied from left to right. For the double and triple box tunnels, the plastic hinge initially develops at positions A or C. As reported earlier, plastic hinges at the interior columns do not developed until the plastic hinges at the four corners of the outer frame are developed. The sequence of the plastic hinge formation is different due to differences in the stiffness ratio between the structural members and supporting soil springs for various soil conditions. Consequently, the moment distributions are different. Figures 14 and 15 show the bending moment diagrams of the single box tunnel at different damage states for $V_s = 50$ m/s and $V_s = 400$ m/s. It is observed that the moment distributions are different for the two cases where sequences of the plastic hinge formation are different.

It should be noted that any plastic hinge formation in the middle of the frame element is not observed in Figs. 14 and 15, even though the computational model is capable of simulating it. It is also observed that the plastic hinge formation does not dramatically change the bending moment distributions. Even though the sectional moment–curvature

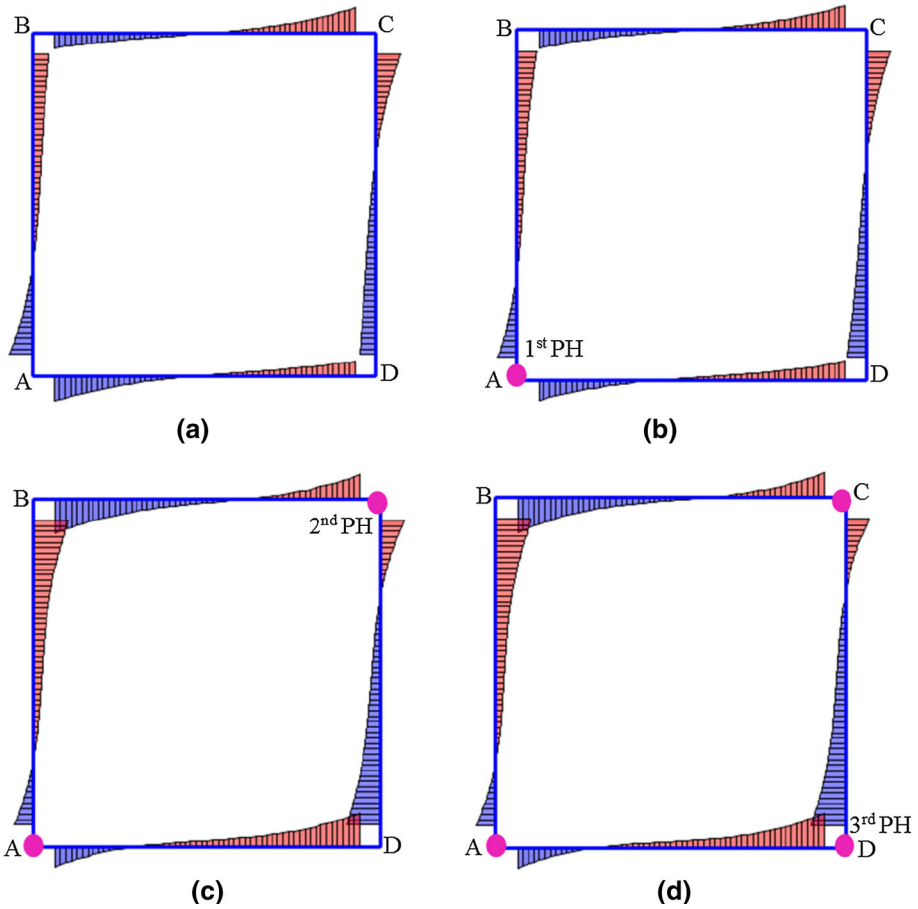


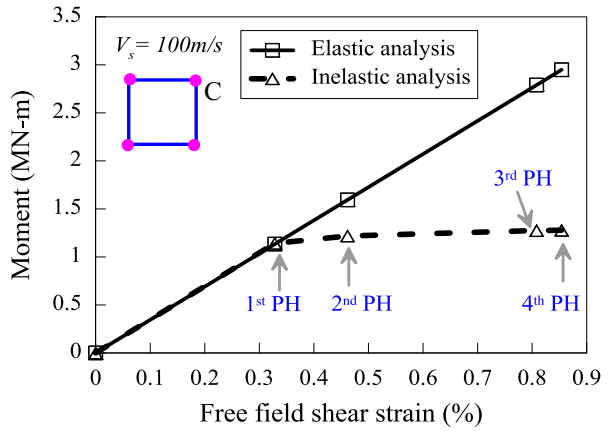
Fig. 15 Bending moment diagrams of single box tunnel, $V_s = 400$ m/s. **a** Elastic range, **b** after 1st plastic hinge is formed, **c** after 2nd plastic hinge is formed, **d** after 3rd plastic hinge is formed

relations show a softening behavior as shown in Fig. 5, the cross sections are ductile enough such that the softening phase is not reached before the plastic hinges are formed at all corners.

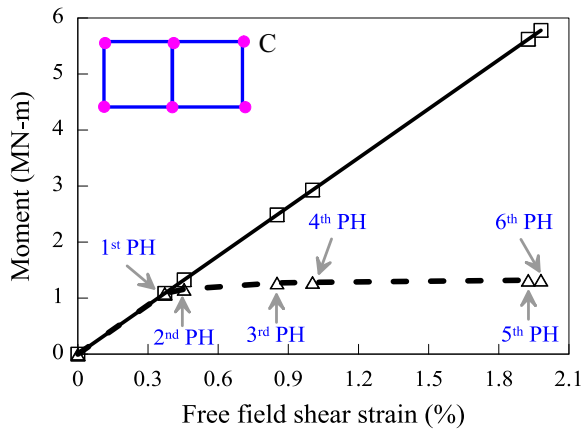
4.2 Comparison between elastic and inelastic analysis

An inelastic analysis makes it possible to estimate the level of damage of the structure, which is crucial for the performance-based seismic design. However, it is seldom performed in practice to determine the seismic response of tunnels, primarily due to difficulties in performing the analysis. It would be useful if corresponding elastic moment is determined such that the damage level can be estimated from elastic analyses. We performed parallel elastic analyses and computed the moments induced in the tunnel structure. Figure 16 compares the nonlinear capacity curve and the elastic moment response at the top-right corner section of the wall (C' s in Fig. 13) of the single, double and triple boxes for $V_s = 100$ m/s. Triangular markers on the nonlinear capacity curve represent the

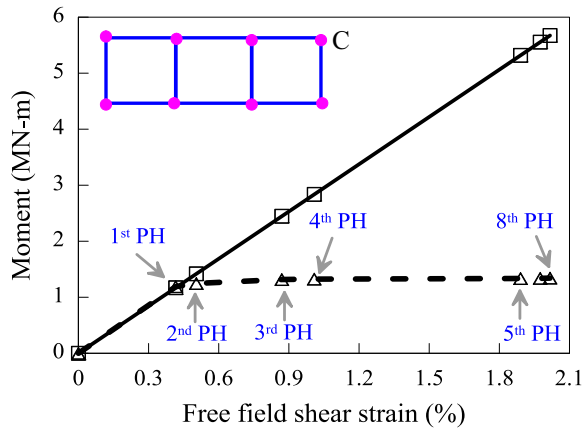
Fig. 16 Comparison of elastic and inelastic behaviors at the point C (*top-right* corner section): **a** single box, **b** double box and **c** triple box tunnel



(a)



(b)



(c)

inelastic moments and induced shear strains at which plastic hinges develop within the tunnel structure, whereas rectangular markers on the elastic curve represent corresponding elastic moments. For example, 2800 kN-m is the elastic moment at the free field shear strain at which the fourth plastic hinge forms as shown in Fig. 16a. Similarly, 5400 and 5500 kN-m are the elastic moments corresponding to the sixth and the eighth plastic hinges of the double and triple box tunnels, respectively.

From Fig. 16, it is observed that the elastic moments at the top-right corner section of the single, double, and triple box tunnels are approximately 34, 24 and 13 % larger than the inelastic moments, respectively, at 0.5 % free field shear strain. We performed elastic analyses on all tunnels and soil profiles. The results of the analyses are used to predict the damage level, which are explained in detail in the following section.

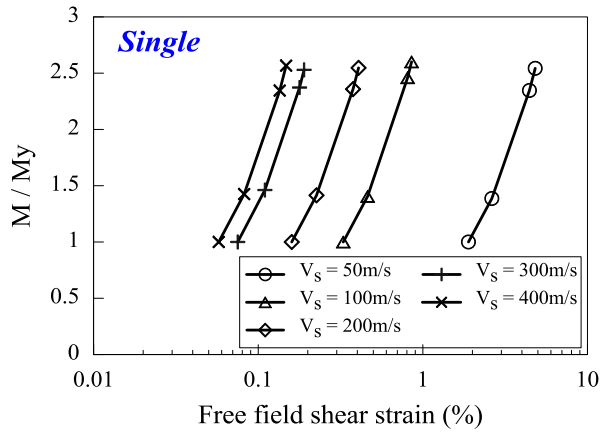
5 Damage analysis

A damage state represents the damage condition of a facility and is associated with a limit state of the mechanical response, often termed as DI. The damage states and corresponding indices of above-ground structures are well defined, but they have not been clearly identified for underground structures. In this section, the damage states of cut-and-cover box tunnels and associated DIs are presented. We propose to use the number of plastic hinges as an indicator of damage level, since we believe that it best reflects the accumulation of damage of a box tunnel structure. Three damage states of cut-and-cover tunnels are classified, which are minor/slight, moderate, and extensive. The collapse damage state is not defined because a box tunnel is not likely to collapse due to formation of plastic hinges. DI is defined as the ratio of the elastic moment demand to the yield moment (M_y). In all damage analyses, the values of DIs were recorded whenever a new plastic hinge is formed within the structure. Figure 17 shows DIs for various soil conditions and tunnel types. The free field shear strain is presented on a logarithmic scale for a visual efficiency. The damage states, number of plastic hinges (NPH), and corresponding DIs defined in this study are summarized in Table 1.

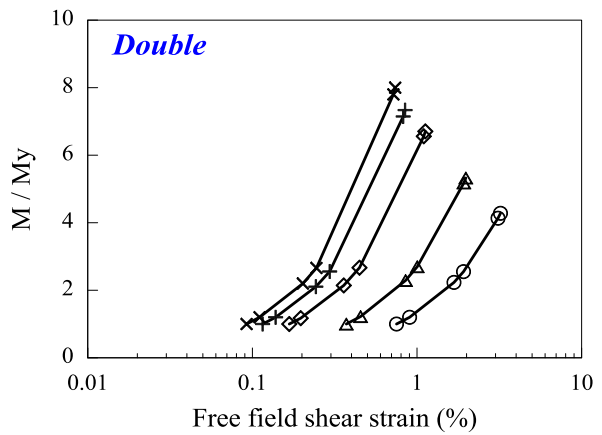
NPH associated with each damage state is identical regardless of the box type, whereas the corresponding DIs are different. The minor/slight, moderate, and extensive damage states initiate when the NPH exceeds one, two, and three, respectively. For the single box tunnel, DIs are almost independent of the stiffness of the soil. The DI ranges from 1.0 to 1.2 for minor/slight damage state, and from 1.2 to 2.0 for the moderate state. The extensive damage state initiates when DI exceeds 2.0. DI corresponding to each damage state is shown to be similar for double and triple box tunnels. As for the single tunnel, it is demonstrated that DI is not highly influenced by the stiffness of the soil until plastic hinges are formed at all outer corners (NPH = 4). At higher NPH, DI is shown to vary significantly according to the soil stiffness. DIs for minor/slight and moderate damage states are identical to those of the single box tunnel and range from 1.0 to 1.2 and from 1.2 to 2.0, respectively.

It should be noted that in the design of reinforced concrete structures, M_d is used instead of M_y to account for the uncertainties in the structural capacity. Therefore, when applying the results of this study in design, it is recommended to replace M_y with M_d . In Table 1, DIs proposed by Argyroudis and Pitilakis (2012) for single box tunnels are shown for comparison purposes. The proposed indices are shown to be lower and therefore more conservative than those by Argyroudis and Pitilakis (2012). Since the damage states and

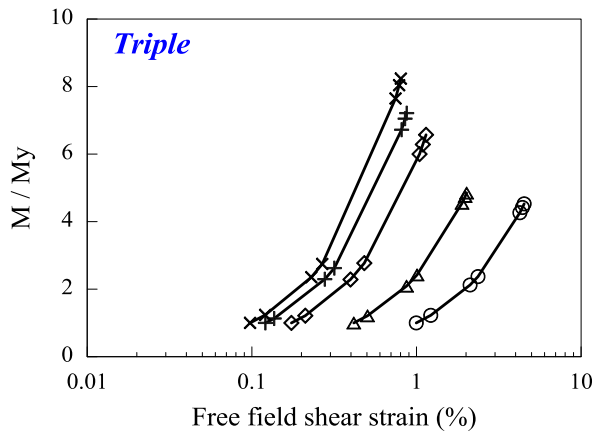
Fig. 17 M/M_y ratios at the formation of plastic hinges: **a** single box, **b** double box and **c** triple box tunnel



(a)



(b)



(c)

Table 1 Proposed definition of damage states, corresponding damage indices, and indices of Argyroudis and Pitilakis (2012)

Tunnel type	Damage state	Number of plastic hinges (NPH)	Damage index (DI, M/M_y)	Damage index (DI_d , M/M_d) (Argyroudis and Pitilakis 2012)
Single box	None	0	$DI < 1.0$	$DI_d < 1.0$
	Minor/slight	$1 \leq NPH < 2$	$1.0 \leq DI < 1.2$	$1.0 < DI_d \leq 1.5$
	Moderate	$2 \leq NPH < 3$	$1.2 \leq DI < 2.0$	$1.5 < DI_d \leq 2.5$
	Extensive	$3 \leq NPH$	$2.0 \leq DI$	$2.5 < DI_d \leq 3.5$
Double box	None	0	$DI < 1.0$	N.A.
Triple box	Minor/slight	$1 \leq NPH < 2$	$1.0 \leq DI < 1.2$	N.A.
	Moderate	$2 \leq NPH < 3$	$1.2 \leq DI < 2.0$	N.A.
	Extensive	$3 \leq NPH$	$2.0 < DI$	N.A.

indices determined in this study are all based on detailed nonlinear inelastic analyses, we believe that the proposed criteria are more representative than previous recommendations. The damage states and the corresponding DIs in Table 1 will be useful in design of cut-and-cover tunnels based on the performance-based design concept.

It should be noted that even though representative metro tunnel sections were selected and used in this study, tunnel sections may differ for different regions. A comprehensive study on the effect of tunnel section on DI is warranted to evaluate its variability. The use of the proposed DIs should be limited to box tunnels with similar dimensions and depth of overburden to those used in this paper.

6 Conclusions

The damage analyses of cut-and-cover tunnels under seismic loading were performed. Typical cut-and-cover tunnels of single, double, and triple box structures designed for metro subway systems in South Korea were selected for this study. The tunnel structures were modeled by nonlinear frame elements with series of normal and shear springs to consider the soil–tunnel interaction. The pushover analyses with the pseudo-static analysis procedure were applied to the tunnels to develop the capacity curves. For each tunnel, the accumulation of damage defined in terms of plastic hinges was monitored. The following conclusions are drawn from the results of the numerical simulations.

- The box tunnel will experience a rigid body rotation and shear deformation (racking) when subjected to earthquake loading. The amount of the rotation and racking depends on the stiffness of the surrounding soil. Significant rigid body rotation is shown to occur for soft soils with V_s less than 100 m/s.
- The sequence of the development of plastic hinges depends on the stiffness ratio of the box tunnel to the surrounding soil. For all tunnels modeled in this study, plastic hinges formed at the inner columns after they developed at all four outer corners.
- The box tunnels do not immediately collapse even when plastic hinges form at all outer corners of the structure, primarily due to the support from the surrounding soil. However, double and triple box tunnels may collapse due to flexural failure when inner column collapses.

- The three damage states of tunnels and associated DIs are proposed. The damage state is defined in terms of NPHs that form in the tunnel structure, because we believe that it best represent the damage accumulated in the structure. DI is defined as the ratio of the elastic moment demand to the yield moment of the structural members of the box tunnel. DIs corresponding to the damage states range from 1.0 to 2.0. We recommend to replace M_y with M_d in using the proposed criteria in a seismic design.

Acknowledgments This research was supported by Basic Science Research Program through the National Research Foundation of Korea (NRF) funded by the Ministry of Science, ICT and Future Planning (NRF-2015R1A2A2A01006129).

References

- An X, Maekawa K (1997) Failure analysis of underground RC frame subjected to seismic actions. *J Mater Concr Struct Pavements Jpn Soc Civ Eng (JSCE)* 36:251–267
- Andreotti G, Lai CG, Martinelli M (2013) Seismic fragility functions of deep tunnels: a new cumulative damage model based on lumped plasticity and rotation capacity. Paper presented at the ICEGE Istanbul, Turkey
- Argyroudis S, Ptilakis K (2012) Seismic fragility curves of shallow tunnels in alluvial deposits. *Soil Dyn Earthq Eng* 35:1–12
- Bobet A (2003) Effect of pore water pressure on tunnel support during static and seismic loading. *Tunn Undergr Space Technol* 18:377–393
- Chang J, Park D, Kim D-K (2014) Seismic analysis of shallow cut and cover tunnel via frame analysis. *J Korean Geotech Soc* (submitted)
- Dowding CH, Rozan A (1978) Damage to rock tunnels from earthquake shaking. *J Geotech Eng Div* 104:175–191
- Hashash YM, Hook JJ, Schmidt B, John I, Yao C (2001) Seismic design and analysis of underground structures. *Tunn Undergr Space Technol* 16:247–293
- Hashash YMA, Park D, Yao JIC (2005) Ovaling deformations of circular tunnels under seismic loading, an update on seismic design and analysis of underground structures. *Tunn Undergr Space Technol* 20:435–441
- Hashash Y, Karina K, Koutsoftas D, O’Riordan N (2010) Seismic design considerations for underground box structures. Paper presented at the Earth Retention Conference, Washington
- Huo H, Bobet A, Fernández G, Ramírez J (2006) Analytical solution for deep rectangular structures subjected to far-field shear stresses. *Tunn Undergr Space Technol* 21:613–625
- Iai S (2005) International standard (ISO) on seismic actions for designing geotechnical works—an overview. *Soil Dyn Earthq Eng* 25:605–615
- Khani S, Homami P (2014) Seismic performance of shallow underground subway stations in soft soil. *J Eng Geol* 8:1983–2002
- Liu J, Liu X (2008) Pushover analysis of Daikai subway station during the Osaka-Kobe earthquake in 1995. Paper presented at the 14th world conference on earthquake engineering, Beijing, China
- MLTM (2009) Earthquake resistance design regulations for subway structures. Ministry of Land, Transport and Maritime Affairs
- Moehle J, Elwood K, Sezen H (2002) Gravity load collapse of building frame during earthquakes ACI Special Publication 197
- Nakamura S, Yoshida N, Iwatate T (1996) Damage to Daikai subway station during the 1995 Hyogoken-Namvu earthquake and its investigation. JSCE, Committee of Earthquake Engineering
- Owen GN, Scholl RE (1981) Earthquake engineering of large underground structures: final report. The Division; National Technical Information Service
- Park D, Sagong M, Kwak DY, Jeong CG (2009) Simulation of tunnel response under spatially varying ground motion. *Soil Dyn Earthq Eng* 29:1417–1424
- Parra-Montesinos GJ, Bobet A, Ramirez JA (2006) Evaluation of soil–structure interaction and structural collapse in Daikai subway station during Kobe earthquake. *ACI Struct J* 1:113–122
- Penzien J (2000) Seismically induced racking of tunnel linings. *Int J Earthq Eng Struct Dyn* 29:683–691
- Sharma S, Judd WR (1991) Underground opening damage from earthquakes. *Eng Geol* 30:263–276

- Wang JM (1985) The distribution of earthquake damage to underground facilities during the 1976 Tangshan earthquake. *Earthq Spectra* 1:741–757
- Wang JN (1993) Seismic design of tunnels: a state-of-the-art design approach. Monograph 7, Parsons Brinckerhoff Quade & Douglas, Inc., New York
- Wang Z, Zhang Z (2013) Seismic damage classification and risk assessment of mountain tunnels with a validation for the 2008 Wenchuan earthquake. *Soil Dyn Earthq Eng* 45:45–55
- Wang W, Wang T, Su J, Lin C, Seng C, Huang T (2001) Assessment of damage in mountain tunnels due to the Taiwan Chi-Chi earthquake. *Tunn Undergr Space Technol* 16:133–150
- Yoshimura M, Takaine Y, Nakamura T (2004) Axial collapse of reinforced concrete columns. Paper presented at the 13th world conference on earthquake engineering, Vancouver, BC, Canada